LANGMUIR Article
Cite This: Langmuir 2019, 35, 5608−5616
pubs.acs.org/Langmuir

Redox-Triggered Disassembly of Nanosized Liposomes Containing Ferrocene-Appended Amphiphiles

William L. Odette, Nicholas A. Payne, Rustam Z. Khaliullin,* and Janine Mauzeroll*

Department of Chemistry, McGill University, 801 Sherbrooke Street West, Montreal, Quebec H3A OB8, Canada

Supporting Information

ABSTRACT: We report a redox-responsive liposomal system capable of oxidatively triggered disassembly. We describe the synthesis, electrochemical characterization, and incorporation into vesicles of an alternative redox lipid with significantly improved synthetic efficiency and scalability compared to a ferrocene-appended phospholipid previously employed by our group in giant vesicles. The redox-triggered disassembly of both redox lipids is examined in nanosized liposomes as well as the influence of cholesterol mole fraction on liposome disassembly and suitability of various chemical oxidants for *in vitro* disassembly experiments. Electronic structure density functional theory calculations of membrane-embedded ferrocenes are provided to characterize the role of charge redistribution in the initial stages of the disassembly process.

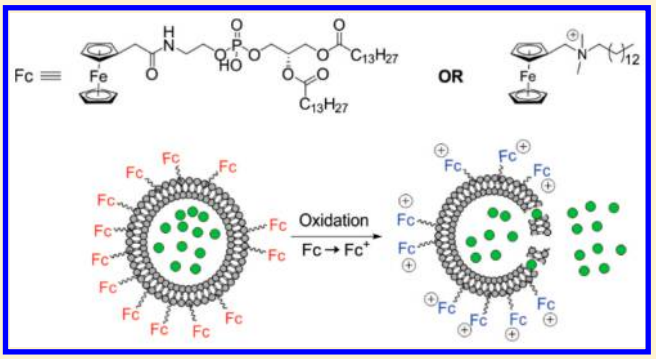

1. INTRODUCTION

Liposomes (lipid bilayer vesicles) have been the subject of intense study as carrier vehicles in biological systems since their first description nearly 60 years ago.[1] The intrinsic biocompatibility of liposomes has led to their investigation for a wide range of potential applications from cosmetics[2] to diagnostic imaging,[3] but the majority of efforts has focused on liposomes as drug delivery systems, particularly with regard to cancer. While liposomes comprise a significant fraction of currently approved nanodrugs,[4,5] this observation belies the challenge implicit in bringing a model system from the bench to the clinic, especially for liposomes containing non-naturally derived synthetic elements. This work investigates whether liposomes containing phospholipids bearing redox-active ferrocene "headgroups" will display comparable redox-triggered disassembly behavior in the ∼100 nm size range (the most relevant for application as biological nanocarriers) as was previously observed for micron-sized vesicles.[6] We describe the effect of cholesterol addition on redox liposomes and the disassembly of vesicles containing a simple ferrocene-functionalized quaternary ammonium amphiphile, a compound of great interest as a redox-active moiety due to the simplicity and scalability of its preparation. The electrochemical behavior of both redox lipids is also examined in simplified systems to address the question of whether the observed disassembly is in fact the result of a straightforward one-electron oxidation of the ferrocene headgroup.

Our initial report[6] relied on giant vesicles (diameter 1−100 μm), an attractive model membrane system due to their suitability for observation by optical microscopy, facilitating the direct observance of morphological changes (i.e., oxidation-triggered disassembly) in real time. Because of their large radius and low curvature, giant vesicles are preferable to large (∼80−1000 nm) or small (≤80 nm) vesicles as biologically relevant planar membrane models,[7] but their size and unscalable methods of preparation[8] render them unsuitable as drug carriers, where the optimal size to prolong circulation time and minimize macrophage clearance is on the order of about 100−300 nm.[9] Furthermore, the enhanced permeability and retention (EPR) effect—a consequence of aberrant tumor vasculature[10] frequently invoked as a design principle for nanodrugs—has recently been shown[11−13] to be an inconsistent predictor of the biodistribution and efficacy of liposomal drug formulations. Nevertheless, there are many potential workarounds to this setback. In the clinical research setting, further understanding of the heterogeneity of tumor tissue as well as the development of model systems more closely resembling the milieu of human tumors[14] will facilitate the evaluation of liposomal drug delivery systems (DDS) in EPR-susceptible cancers. At the level of fundamental research, the incorporation of targeting or stimulus-responsive functionalities into liposomes[15] will enhance the efficacy of delivery compared to passively targeted accumulation via the EPR effect. We may then suppose that the future of stimulus-responsive nanomedicine lies in the realm of tailored therapeutics, i.e., the matching of a targeted or stimulus-responsive nanocarrier to a particular pathology that will afford the necessary stimulus or targeting element to realize the

Received: December 24, 2018
Revised: March 19, 2019
Published: March 27, 2019

DOI: 10.1021/acs.langmuir.8b04267
Langmuir 2019, 35, 5608−5616

benefits of the targeted DDS. Since we represent merely one link in a long chain reaching from the bench to the clinic, it is incumbent on us to develop—at the level of fundamental physicochemical principles—the most refined understanding possible of the mechanisms governing stimulus-responsive delivery vehicles such that we can explain and contextualize *post hoc* the behavior of such a system as the complexity of its environment is increased toward the ultimate goal of use in humans. In translating our redox-responsive giant vesicle system to a nanosized liposomal system, we have increased membrane curvature by reducing the size of the vesicle. While it is straightforward to assert that the energy of a spherical vesicle increases with decreasing vesicle diameter,[16] we cannot predict—with any measure of scientific rigor—the effect of the altered lateral pressure profile[17,18] of a ∼100 nm diameter redox liposome (compared to a giant vesicle with diameter ≥1 μm) on its oxidatively triggered disassembly. It is therefore necessary to verify this behavior in the course of physical characterization of nanosized redox-active liposomes before further investigation of their biophysical properties and development of a mechanistic model of the membrane dynamics leading to disassembly.

A thorough understanding of the mechanistic basis (i.e., the biophysical phenomena governing disassembly) of such stimulus-responsive nanocarriers is necessary to improve our ability to predict and contextualize () observed behavior in biological systems. Membrane phenomena leading to vesicle breakdown are well-understood in pH-responsive systems,[19−21] but poorly characterized for redox-responsive vesicles.[22] Despite the relative paucity of high-quality studies[23,24] concerning the mechanism of disassembly of redox-responsive liposomal systems, there is much useful information to be gleaned from the extant literature in the process of developing a testable model of oxidatively triggered liposome disassembly. Moreover, a fundamental characterization of the molecular mechanism of the observed oxidatively triggered disassembly may prove generally useful for the understanding of membrane-bound electron transfer processes.[25,26]

2. EXPERIMENTAL SECTION

2.1. Chemicals. 1,2-Distearoyl-*sn*-glycero-3-phosphocholine (DSPC), 1,2-distearoyl-*sn*-glycero-3-phospho-(1′-*rac*-glycerol) (DSPG), 1,2-dimyristoyl-*sn*-glycero-3-phosphocholine (DMPC), and cholesterol were purchased from Avanti Polar Lipids, Inc. 1,2-Dimyristoyl-*sn*-glycero-3-phosphoethanolamine (DMPE), potassium hexachloroiridate (III/IV), ceric ammonium nitrate, 1-ethyl-3-(3-(dimethylamino)propyl)carbodiimide hydrochloride (EDC-HCl), and ferrocenemethanol were purchased from Sigma-Aldrich. KCl was purchased from ACP, Montreal, Canada. Frémy's salt ($K_2NO(SO_3)_2$) was prepared according to a published procedure.[27] Solvents (HPLC grade), sodium and potassium chloride, and trimethylamine (Et_3N) were purchased from Fisher Scientific. All aqueous solutions were prepared with ultrapure water from a Milli-Q reference purification system (EMD Millipore).

2.2. Preparation of Liposomes. All lipids used in liposome preparation were dissolved in chloroform at a concentration of 20 mg/mL (total lipid 5 μmol) in a clean 15 mL glass vial, and solvent was removed by rotary evaporation, leaving a thin film of lipid residue on the flask wall. Vials were left under high vacuum for a minimum of 4 h to remove residual chloroform. Lipid films were taken up in warm *tert*-butanol, frozen in liquid nitrogen, and lyophilized overnight. A 1 mL portion of hydration buffer (typically 215 mM sucrose) heated to 60 °C was added to the flask, and the suspension was agitated on a vortex mixer to give a uniform milky suspension of multilamellar vesicles (MLVs). MLV dispersions were subjected to 3 freeze/thaw (liquid N_2/60 °C H_2O bath) cycles before extrusion to ensure optimal hydration. MLVs were loaded into a mini-extruder (Avanti Polar Lipids) equipped with two stacked 19 mm diameter polycarbonate filters (Sigma-Aldrich). Lipids were subjected to 21 passes through 200 nm filter membranes and stored at 4 °C.

2.3. Photon Correlation Spectroscopy. Size determination of liposomes was performed on a Brookhaven 90Plus multiangle particle sizer equipped with a 685 nm 35 mW solid-state laser. All data were acquired with Brookhaven particle size analysis software (v5.29), and plots were constructed using an in-house MATLAB script. A 25 μL aliquot of liposome suspension was added to a glass cuvette and the volume adjusted to provide an appropriate count rate (total volume 2 mL, ∼10^5 cps). Measurements were performed at room temperature (ca. 23 °C) with a 90° detection angle and a dust cutoff value of 30 nm. Each measurement was performed in triplicate, and the values were averaged.

2.4. Lipid Quantitation. Total lipid content was quantified using the method of Stewart.[28] All samples were analyzed in triplicate. Briefly, 10 μL of liposomes was added to a dry test tube (13 × 100 mm). A 2 mL portion of chloroform was added followed by an equivalent amount of ammonium ferrothiocyanate (0.4 M NH_4SCN, 0.1 M $FeCl_3$). The biphasic mixtures were agitated for 20 s using a vortex mixer and centrifuged at 1500 rpm for 5 min. An aliquot (500 μL) of the chloroform layer was removed and the absorbance read at 488 nm. By maintaining consistent volume across standard and experimental samples, molar lipid quantities were then calculated using previously established calibration curves.

2.5. Synthesis of Ferrocenylated Phospholipid (FcDMPE). Ferrocene-appended phospholipid **1** was prepared as previously reported[6] with slight modifications. Ferroceneacetic acid (9.98 mg, 0.0409 mmol), EDC-HCl (10.13 mg, 0.0491 mmol), and Et_3N (13 μL, 0.09 mmol) were dissolved in dry dichloromethane (3 mL) cooled to 0 °C in a flame-dried round-bottom flask equipped with a reflux condenser. The solution was stirred for 15 min, and DMPE (20 mg, 0.0315 mmol) was added dropwise as a solution in dichloromethane (DCM; 2 mL). The solution was allowed to warm to room temperature and subsequently heated to 40 °C. The reaction progress was monitored by thin-layer chromatography ($CHCl_3$:MeOH:H_2O 65:25:4) for the consumption of starting material. Upon completion (ca. 2 h) solvent was removed by rotary evaporation, and the residue was dissolved in a minimal amount of DCM (approximately 0.2 mL) and purified by preparative thin-layer chromatography on boric-acid-impregnated plates ($CHCl_3$:MeOH:H_2O 65:25:4) to afford a golden oil (21 mg, 81%). Purified phospholipid was filtered three times through a cotton plug to remove residual silica particles. ^{1}H NMR (500 mHz, $CDCl_3$): δ 12.4 (br, 1H), 7.03 (br, 1H), 5.23 (br, 1H), 4.39−4.37 (br, 1H), 4.23 (br, 2H), 4.13−4.10 (br, 5H), 3.94 (br, 2H), 3.48 (br, 2H), 3.29 (br, 2H), 3.07 (br, 4H), 2.32−2.28 (m, 4H, *J* = 6.7 Hz, 12.5 Hz, 4H), 1.60 (br, 4H), 1.27 (br, 40H), 0.90−0.88 (t, *J* = 6.6 Hz, 6H). HRMS (−ESI): $(M - H)^-$ calcd for $C_{45}H_{75}FeNO_9P$, 860.45343; found, 860.45477.

2.6. Synthesis of *N*,*N*-Dimethyl(ferrocenylmethyl)-tetradecylammonium bromide (FTDMA). **2** was prepared according to the procedure of Saji et al.[29] with slight modifications. Equimolar amounts of neat ((*N*,*N*-dimethylamino)methyl)ferrocene and *n*-tetradecyl bromide were mixed and heated to 60 °C. A small portion (ca. 3 mL) of dry acetone was added to the mixture to ensure homogeneity, and the reaction was stirred for 2 h, forming a viscous red−brown oil. The residue was recrystallized twice from boiling acetone to afford the yellow crystalline product (65%). ^{1}H NMR (500 mHz, $CDCl_3$): δ 4.87 (s, 2H), 4.53 (t, *J* = 1.9 Hz, 2H), 4.36 (br, 2H), 4.31 (br, 5H), 3.38−3.34 (m, 2H), 3.27 (s, 6H), 1.74 (br, 2H), 1.35 (br, 4H), 1.27 (br, 18H), 0.91−0.88 (t, *J* = 7 Hz, 3H). ^{13}C NMR (126 MHz, $CDCl_3$): δ 72.2 (s), 72.1 (s), 70.6 (s), 69.6 (s), 65.3 (s), 63.1 (s), 49.8 (s), 31.9 (s), 29.7 (s), 29.64 (s), 29.58 (s), 29.45 (s), 29.41 (s), 29.36 (s), 29.25 (s), 26.35 (s), 22.9 (s), 22.7 (s), 14.1 (s). HRMS (+ESI): (M^+) calcd for $C_{27}H_{46}FeN^+$, 440.2974; found, 440.2977. IR ν_{max}: 2916, 2849, 1469, 1028, 1001, 891, 870, 847, 808, 517, 495, 485 cm^{-1}. mp 140 °C.

DOI: 10.1021/acs.langmuir.8b04267
Langmuir 2019, 35, 5608−5616

2.7. Redox-Triggered Liposome Disassembly. Redox and nonredox liposomes were prepared using 215 mM sucrose as the hydration buffer and characterized as described above. A 750 μL aliquot of oxidant (1,4-benzoquinone, potassium nitrosodisulfonate, K_2IrCl_6, $(NH_4)_2Ce(NO_3)_6$, 1−10 mM aqueous solution) was freshly prepared and immediately added to the liposome dispersion, and changes in size and polydispersity index were monitored by dynamic light scattering (DLS) immediately after the addition of oxidant and at t = 15, 30, 45, 60, 120, 180, and 240 min postaddition as well as overnight.

2.8. Electrochemistry/Cyclic Voltammetry. Electrochemical measurements were carried out with a PG340 bipotentiostat on either an ElProscan 1 or ElProscan 3 system. Cyclic voltammetry was performed with either a Pt microelectrode of diameter 25 μm (RG = 3) fabricated in-house[30] or a glassy carbon disk electrode (3 mm diam, CH Instruments, Austin, TX). A Ag/AgCl reference electrode (CH Instruments, Austin, TX) and a Pt wire as counter electrode (0.5 mm diam, 99.99%, Goodfellow Cambridge Limited, Huntingdon, England) completed the electrochemical cells. Measurements in chloroform were performed with a Pt microelectrode and Ag wire (1 mm diam, annealed 99.99%, Goodfellow) as a quasireference/counter electrode. Cyclic voltammograms were acquired at 20 mV/s with the Pt microelectrode and at 100 mV/s with the glassy carbon electrode. Aqueous measurements were performed in 0.1 M KCl as supporting electrolyte while 0.1 M TBAPF6 was used in acetonitrile.

2.9. Computer Modeling. For the investigation of the effect of the oxidation state of the ferrocene group on the structure of the lipid bilayer, a simplified atomistic model of the membrane was created, and its structure was optimized using density functional theory (DFT). In the first step, optimal atomic positions of a DMPC molecule in a two-dimensional periodic layer were found. The area per lipid molecule, determined in previous molecular dynamics simulations,[31] was fixed at 65 Å^2 per molecule. In the next step, a 3 × 3 supercell of the DMPC lattice was created, and one of the nine DMPC molecules was modified to include the ferrocene group. This produced a model of FcDMPE molecules uniformly distributed in the DMPC lattice with the 1:8 FcDMPE:DMPC ratio. A number of initial conformations of the Fc chain were considered resulting in various optimized positions of the ferrocene group relative to the layer (e.g., extended above the choline groups or embedded in them). To make DFT calculations of the electronic structure of nine lipid molecules feasible, the long alkane chains $C_{13}H_{27}$ in the lipids were replaced with shorter C_2H_5 groups. It was verified that this replacement does not affect the electronic structure of the head groups to a noticeable degree. The carbon atoms at the end of the alkyl chains were restrained during the structure optimization at their original positions in the lattice. This constraint was introduced to retain the forces exerted by the intertwined alkyl chains on the headgroups. It was verified that this constraint has negligible effect on final results. The effect of the aqueous environment was modeled with the self-consistent continuum solvation method[32] with the dielectric constant set to 78. All structures were optimized in the reduced state of the ferrocene group. The optimal structures were then used as a starting geometry in the optimization of the oxidized state. It was determined that the doublet spin state has the lowest energy for all oxidized configurations.

All calculations were performed using the DFT module of the CP2K software package. In the dual Gaussian and plane-wave scheme implemented in CP2K,[33] a double-ζ Gaussian basis set with one set of polarization functions (DZVP)[34] was used to represent molecular orbitals. A plane-wave cutoff of 300 ~ Ry was used to represent the electron density. Separable norm-conserving Goedecker−Teter−Hutter pseudopotentials were used to describe the interactions between the valence electrons and ionic cores,[35,36] and the Brillouin zone was sampled at the Γ point. The Perdew−Burke−Ernzerhof generalized gradient approximation[37] corrected to account for dispersion interactions[38] was used as the exchange-correlation functional. The size of a simulation box along the perpendicular direction to the layer was set to 30 Å to ensure decoupling of the periodic images of the layers.

3. RESULTS AND DISCUSSION

3.1. Synthetic Optimization and Alternate Ferrocene Amphiphiles. A modest increase in the yield of ferrocenyl-DMPE (FcDMPE, **1**) was obtained (81% versus 62%) by employing EDC-HCl as the coupling reagent in place of dicyclohexylcarbodiimide (DCC) (Scheme 1).

Scheme 1. Synthesis of Ferrocene-Phospholipid Conjugate 1 (FcDMPE) and Monoalkylated Ferrocene Amphiphile 2 (FTDMA)

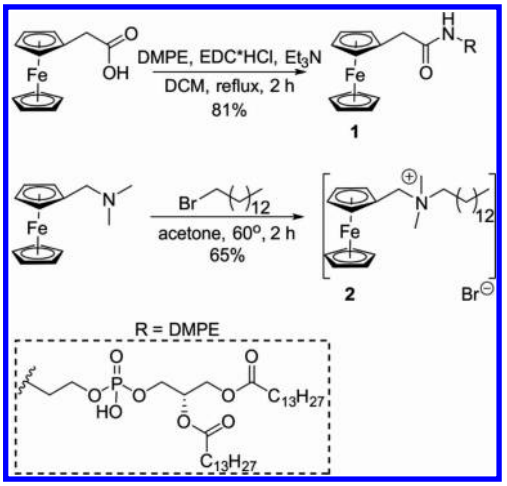

Reaction times (from >12 to ~2 h) and conversion of starting material were also considerably improved compared to our previous method.[6] Despite these improvements, synthetic efficiency—especially with regard to material cost and scalability—will remain an important concern in the long-term application of this system. In addition to such pragmatic concerns, we are also interested in expanding the "toolbox" of redox-active amphiphiles for use in stimulus-responsive self-assembled systems. While the majority of extant redox-responsive assemblies utilize reductively triggered redox moieties such as disulfides and quinones,[39] ferrocene remains relatively unexplored as a reactive functionality in responsive DDS (although ferrocene-modified lipids[40,41] and polymers[42] have found recent applications as transfection and gene delivery agents) despite the advantages afforded by its chemical stability, orthogonality to native biochemical redox reactions, and the highly reproducible electrochemical behavior of the ferrocene/ferrocenium redox couple.

A pair of cationic monoalkyl ferrocene derivatives were reported by Saji[29,43] in an early example of redox-sensitive self-assembled structures. In observing these compounds, we wondered if the redox-triggering behavior seen with a ferrocene-appended phospholipid could be recapitulated with a simple cationic amphiphile, that is, whether the gross structural features (hydrocarbon tail, polar head with pendant ferrocene) of FcDMPE are sufficient to reproduce oxidatively triggered disassembly. We opted to employ an analogue with the ferrocene moiety proximal to the cationic ammonium to approximate the relative positions of the polar headgroup and ferrocene in FcDMPE. We also incorporated a C_{14} alkyl chain in place of the originally reported C_{11} to reduce the degree of hydrophobic mismatch in the bilayer. The preparation of **2** was found to be more straightforward, economical (atom- and penny-wise), and scalable than that of phospholipid **1**.

DOI: 10.1021/acs.langmuir.8b04267
Langmuir 2019, 35, 5608−5616

3.2. Electrochemical Characterization of Redox Lipids. To evaluate the hypothesis that liposome destabilization results from ferrocene oxidation effected by Frémy's salt, we opted to start with a lipid analogue to facilitate the measurement. FcMeOH was selected because of its well-characterized electrochemical response and good water solubility for the reaction with Frémy's salt. Furthermore, the standard potential was very close to that of the lipids tested (E° = 0.21 V versus Ag/AgCl[44]).

To study the electrochemical reaction, we spiked a solution of 1 mM FcMeOH with a 1 mM solution of Frémy's salt in 0.1 M KCl in addition to a blank, spiked with 0.1 M KCl. We noted an immediate color change (<1 s) from pale yellow to pale green/blue likely due to formation of $[FcMeOH]^+$. We performed cyclic voltammetry with a microelectrode as the diffusion-limited current is linearly proportional to the concentration, and we could determine the extent of conversion and therefore the reaction stoichiometry. A significant downward translation of the voltammograms (Figure 1a) could be observed, which can be explained to be due to the change in bulk concentration ratio of Fc/Fc^+ and not to the presence of Frémy's salt. The steady state currents revealed a final concentration of 0.24 ± 0.01 mM $FcMeOH^+$ (Figure 1a, inset) which corresponds to a reaction requiring 2 equiv of Frémy's salt, suggesting the dimeric form acts as the oxidant.

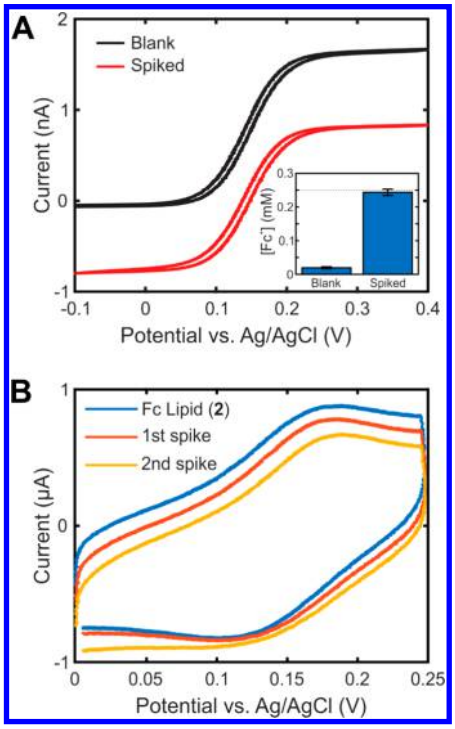

Figure 1. (A) Cyclic voltammetry of FcMeOH showing the effect of spiking with Frémy's salt (1:1) (inset: peak reductive currents of 1 mM FcMeOH spiked with Frémy's salt (red trace) or 0.1 M KCl (black trace). (B) Cyclic voltammetry of FTDMA illustrating the effects of spiking with Frémy's salt.

Unlike FcDMPE, FTDMA is sparingly soluble in aqueous solution, and the direct oxidation of the lipid can be observed electrochemically. We switched to a glassy carbon electrode (3 mm) for this purpose because of the evident fouling of the platinum microelectrode. Here we spiked a 2.5 mM aqueous solution of FTDMA with a small volume of a highly concentrated solution of Frémy's salt (0.25 M) and performed cyclic voltammetry before and after (Figure 1b). A prior scan rate analysis and the linearity of the peak current with the root of the scan rate ensured we were measuring diffusing solution species. A much less pronounced change in the macroelectrode voltammograms was observed; nevertheless, the expected downward translation of the currents could be observed. Again, the downward translation is due to the change in the bulk concentration ratio of $FTDMA/FTDMA^+$ demonstrating that Frémy's salt does indeed directly oxidize the FTDMA lipid.

3.3. Downsizing of Redox-Active Giant Vesicles. Giant vesicles, while conveniently observable by optical microscopy, are too large to be suitable for drug delivery applications *in vivo*—the original intended use of this system—and their methods of production are not scalable. Representative size distributions of redox-active liposomes compared to redox giant vesicles are shown in Figure 2a (passed through a 0.1 μm membrane filter to remove very large particles).

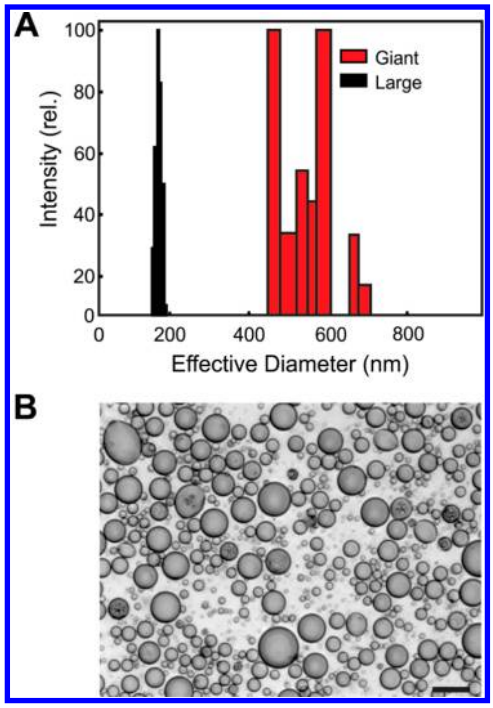

Figure 2. (A) Typical size distributions of redox-active giant and large vesicles obtained from laser light scattering. (B) Optical micrograph of ferrocene-containing giant vesicles (scale bar = 50 μm).

To address this limitation, we adapted our procedure for the production of redox-active giant vesicles to be amenable to the scalable production of liposomes within the size range appropriate for the physiological environment (~80−200 nm). We elected to employ the film hydration−extrusion method of liposome preparation[45,46] as it presents a simple approach to generate monodisperse populations of liposomes, and extruders are commercially available accommodating bench- to commercial-scale production.[47,48] Multilamellar vesicles (MLV) are formed by hydration of a thin lipid film on the walls of a round-bottom flask. In the case of mixed lipid preparations, especially those containing cholesterol,[49] crystallization of individual lipid species may occur during rotary evaporation leading to heterogeneity in the lipid film. To

DOI: 10.1021/acs.langmuir.8b04267
Langmuir 2019, 35, 5608−5616

address this concern, we employed the additional step of dissolving lipid films in *t*-BuOH and lyophilizing to give a more homogeneous "cake" of desiccated lipids. Hydration of this lipid cake affords MLV which may then be converted to liposomes by extrusion. Lipid compositions employed in this study are shown in Figure 3. The key difference in lipid

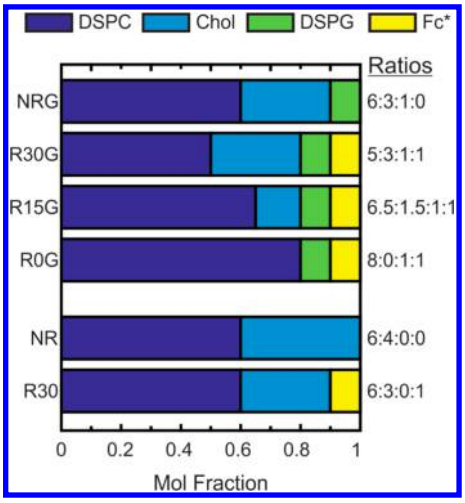

Figure 3. Liposomal lipid compositions employed in this study. Fc* may refer to either FcDMPE or FTDMA.

mixtures employed in this study is the presence or absence of the anionic lipid DSPG. DSPG was included originally to maintain fidelity with the composition of the previously described giant vesicle system (corresponding to composition "$R0_G$"), but once the redox-triggered disassembly was verified for DSPG-containing compositions, we next examined whether the presence of the anionic lipid was necessary for disassembly (discussed in section 3.4).

3.4. Redox-Triggered Liposome Disassembly. We previously showed[6] the rapid disaggregation of ferrocene-containing giant vesicles in response to the addition of a 1 mM solution of hexachloroiridate(IV) while no effect was observed upon treatment with hexachloroiridate(III). Having altered the physical properties (i.e., the imposition of a higher degree of membrane curvature) of the redox liposomes in transitioning from giant (average diameter >1 μm) to large (average diameter ~100 nm) vesicles, we revisited the question of (1) the recapitulation of this so-called "redox popping" behavior and its dependence on lipid composition, and (2) appropriate chemical oxidants to verify the redox-triggered destabilizing effect. Ir(IV) as K_2IrCl_6 (+0.91 V versus Ag/AgCl[50]) did not induce any significant or reproducible degradation of DSPG-containing liposomes (FcDMPE or FTDMA) at concentrations up to 10 mM. In FTDMA-containing liposomes lacking DSPG (compositions "NR" and "R30"), a modest size increase was observed for 1 and 5 mM Ir(IV) (Figures S14–S16). Interestingly, in FcDMPE-containing liposomes, 1 mM produced the greatest size increase, while higher concentrations of iridium resulted in only a marginal increase (Figures S28–S30). Ce(IV) was also evaluated (as $(NH_4)_2Ce(NO_3)_6$, +0.77 V versus Ag/AgCl[51]) but did not produce any effect on either redox-active or control liposome populations up to 10 mM. 1,4-Benzoquinone (BZQ, +0.5 V versus Ag/AgCl[52] for 2e reduction to hydroquinone) was also tested as one example of a "biologically relevant" oxidant and did not produce any effect on redox-active or control liposome populations. While quinones[53] are important biological redox functionalities and are known to be capable of oxidizing ferrocene,[54] the half-wave potential for the reduction of 1,4-benzoquinone to the semiquinone radical anion depends strongly on solvent and substituent conditions.[55] It may therefore be reasonable to envision quinones more as a potential indirect source of ferrocene oxidation in biological media through the generation of the superoxide anion[56] and its subsequent dismutation to a hydroxyl radical (the most strongly oxidizing[57] species in the biological environment) than as directly oxidizing ferrocene. Detailed comparisons (changes in hydrodynamic radius and polydispersity) for each oxidant and lipid composition are shown in Figures S7–S38. Ultimately, Frémy's salt (+0.41 V versus Ag/AgCl[58]) at 10 mM was found to reproducibly induce disaggregation of redox liposomes without impacting the stability of nonredox control populations (Figure 4A-B).

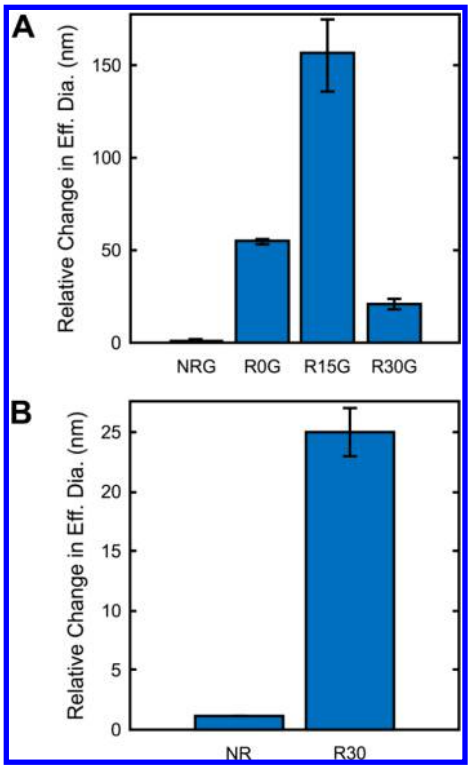

Figure 4. Relative changes in hydrodynamic radius of redox liposomes containing FcDMPE (10 mol %) at t = 4 h postaddition of Frémy's salt: (A) NRG, R0G, R15G, and R30G; (B) NR and R30.

Frémy's salt—potassium nitrosodisulfonate—does not exist in biological systems. It may be reasonably considered, however, to serve as an analogue of nitroxyl (HNO, reduced forms of •NO) compounds, a relatively unexamined class of reactive oxygen/nitrogen species (RONS) in cells that are thought to be capable of acting in either oxidative or reductive capacities.[59,60] This observation may then serve as a starting point for further investigation into which species may actually effect liposome-bound ferrocene oxidation in the cellular environment, a necessary step in defining the pathway to *in vivo* applications of redox liposomes. In FcDMPE-containing preparations with less than 30 mol % cholesterol, significant vesicle disassembly was apparent within minutes of oxidant addition; at a cholesterol content of 30 mol % (compositions "R30" and 'R30G'), breakdown was observed at ca. 2–4 h after oxidant addition. In gel-phase membranes, cholesterol

DOI: 10.1021/acs.langmuir.8b04267
Langmuir 2019, 35, 5608–5616

increases fluidity, while in liquid crystalline membranes, it exerts a rigidifying effect.[61] These experiments are conducted at room temperature with predominantly long-chain (C_{18}) lipids having a main gel−liquid crystalline transition temperature of 55 °C.[62] The observed trend for FcDMPE-containing liposome populations—that increasing the cholesterol fraction lengthens the time course over which disassembly is observed (Figure 4A)—is therefore consistent with the increase of fluidity expected from cholesterol addition to gel-phase membranes.

Interestingly, this trend is not reproduced in FTDMA-containing liposome populations (Figures S13 and S20), in which no significant disassembly is observed in preparations containing less than 30 mol % cholesterol. As the lipid compositions are otherwise identical, these results suggest that the specific mechanism of disassembly is influenced by the nature of the redox functionality and oxidant as well as the liposomal lipid composition. As a control experiment to evaluate the effect of the hydrophobic mismatch between ferrocene lipids (C_{14} acyl chain length) and the bulk membrane lipids (C_{18} acyl chain length) and its potential effect on oxidatively triggered liposome disassembly, oxidant screening was carried out using pseudo-redox-active lipid compositions in which the ferrocene lipid (in both cases) was substituted with 1,2-dimyristoyl-*sn*-glycero-3-phosphocholine (DMPC). No significant size change was observed across all lipid concentrations and oxidants, suggesting that the acyl chain mismatch of ferrocene lipids and membrane constituent phospholipids does not play a significant role in their redox-triggered disassembly. Additionally, electronic structure density functional theory (DFT) calculations were carried out on a simplified model system consisting of a ferrocene-appended phospholipid embedded in a DMPC lattice (Fc:DMPC ratio 1:8) in both ferrocene oxidized and reduced states (see Figure 5A and section 2.9 for details). For the chain conformer, in which ferrocene is extended above the plane of choline headgroups, the difference in the optimized structures of oxidized and reduced states was found to be negligible. Furthermore, the forces on the fixed alkyl atoms were found to be the same in the oxidized and reduced states. A similar observation was made for the conformers with the ferrocene group embedded deeper in the hydrophilic region of the membrane. Figure 5B shows that although the atoms of neighbor DMPC lipids tend to be repelled from the oxidized Fe, their displacement does not exceeds 0.15 Å even for those close to the ferrocene group. This computational result, together with the observation that liposomes containing DMPC in place of ferrocene lipids do not disassemble following exposure to any of the oxidants employed in this study, implies that altering the charge state of the headgroup (represented by the DMPC choline moiety in negative controls) is insufficient to induce membrane disassembly. While this result is not surprising for the ferrocene extended above choline groups, it requires a closer examination in the case of an embedded ferrocene group. Analysis of the electron density distribution indicates that 13% of the excess charge in the oxidized state is localized on the iron atom; 50% is delocalized over the atoms of the cyclopentadienyl rings, and the rest is distributed over the remaining atoms of the FcDMPE lipid. This charge delocalization in conjunction with solvent screening appears to be sufficient to reduce the impact of the change in the oxidation state and to induce only minor structural rearrangements around FcDMPE. While DFT

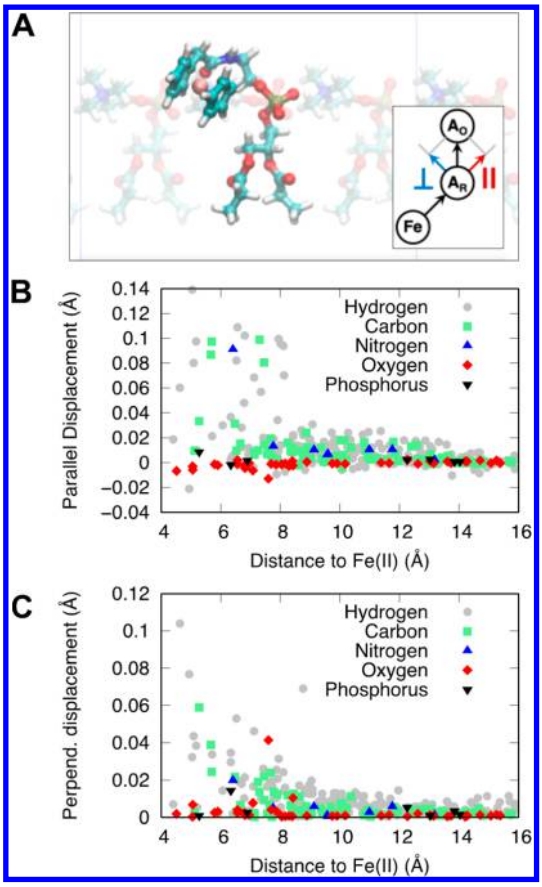

Figure 5. (A) Representative conformation of a ferrocene-appended phospholipid embedded in a DMPC lattice; the inset shows the displacement of atoms of the nearest DMPC neighbors upon oxidation of FcDMPE, and A_R and A_O are the positions of an atom in the reduced and oxidized state, respectively. (B) Parallel components of the displacement vector. (C) Perpendicular component of the displacement vector.

calculations eliminate charge-induced structural rearrangements as the initial stage the of membrane disassembly, further experimental and computational studies are required to investigate the role of membrane curvature, the conformational dynamics of the lipids, diffusion of solvent molecules and ions in the proximity of the oxidation site, aggregation of the ferrocene-functionalized lipids, and their chemical transformations in the disassembly process.

4. CONCLUSIONS

We have demonstrated redox-responsive liposomes prepared in a simple and scalable fashion employing structurally distinct redox functionalities that maintain similar oxidatively triggered disassembly. The suitability of chemical oxidants for *in vitro* vesicle degradation experiments was characterized by light scattering in vesicles and electrochemically to verify the one-electron oxidation of ferrocene by Frémy's salt. Comparable oxidants (with regard to formal potential) such as 1,4-benzoquinone as well as strong oxidants like Ir(IV) and Ce(IV) were found to be unsuitable for this purpose. This observation suggests—as may be intuitively supposed—that thermodynamic parameters such as formal redox potentials are only one variable in the complex picture of oxidation of an organometallic pendant embedded in a phospholipid bilayer. Metal-based oxidants like Ir(IV) and Ce(IV) may function via

DOI: 10.1021/acs.langmuir.8b04267
Langmuir 2019, 35, 5608−5616

several different mechanisms[50,51] depending on reaction conditions and ligand/substrate identities and, likewise, the stepwise electron transfer to afford hydroquinones from 1,4-benzoquinones.[63] Moreover, the data presented for the oxidation of FcMeOH by Frémy's salt suggest a straightforward electrochemical oxidation, which would be distinct from the mechanism proposed for Frémy's salt-induced oxidation of quinones.[64] Inclusion of 10 mol % ferrocene lipid (FcDMPE or FTDMA) was sufficient to reproducibly induce vesicle disassembly, with the time course of vesicle breakdown being lengthened considerably by the inclusion of ca. 30 mol % cholesterol. Non-redox-active liposomes containing DMPC in place of ferrocene lipids did not make evident any disassembly following treatment with oxidizing agents, demonstrating the necessity of the ferrocene unit in the process of oxidatively triggered disassembly. Our study therefore provides the necessary basis of contrast (regarding both the efficacy of oxidants and disassembly trends observed with different redox lipids and overall lipid compositions) and the initial groundwork to begin developing a testable model for the oxidation of bilayer-embedded ferrocene units. Preliminary electronic structure calculations suggest that the addition of positive charge alone (as in the oxidation of ferrocene to ferrocenium) may be a relatively insignificant factor in the membrane disassembly process and highlight the need for more detailed studies of the orientation and conformation of membrane-bound ferrocenes. The development of such a model will carry implications for both the design of redox-responsive nanocarriers and fundamental membrane dynamics, beginning to bridge the gap between bench design of stimulus-responsive delivery systems and their application in biological systems. This study represents an advance of the described redox liposome system with regard to its suitability for *in vivo* studies and an expansion of the redox-active amphiphiles suitable for preparing responsive liposomes. Further studies will focus on the biophysical phenomena underlying oxidatively triggered disassembly as well as the organization and conformation of ferrocene-containing amphiphiles in biomembranes.

■ ASSOCIATED CONTENT

Supporting Information

The Supporting Information is available free of charge on the ACS Publications website at DOI: 10.1021/acs.langmuir.8b04267.

Additional figures including ^{1}H and ^{13}C NMR spectra, FTIR spectra, HRMS spectra, and relative changes in liposome hydrodynamic radii (PDF)

■ AUTHOR INFORMATION

Corresponding Authors

*E-mail: rustam.khaliullin@mcgill.ca.
*E-mail: Janine.Mauzeroll@mcgill.ca.

ORCID

Rustam Z. Khaliullin: 0000-0002-9073-6753
Janine Mauzeroll: 0000-0003-4752-7507

Author Contributions

W.L.O. performed the bulk of the experiments described in the manuscript. N.A.P. assisted in the design and execution of electrochemistry experiments. Computational studies were carried out and analyzed by R.Z.K. The manuscript was written through contributions of W.L.O., N.A.P., R.Z.K., and J.M. All authors have given approval to the final version of the manuscript.

Funding

N.A.P. and W.L.O. were supported by a team operational grant from Fond Quebecois de la Recherche sur la Nature et les Technologies (FRQNT), a contribution from Aligo Innovation. The research is partially funded by the Natural Sciences and Engineering Research Council of Canada through the Discovery Grant (RGPIN-2016-05059). Computational support is provided by Compute Canada.

Notes

The authors declare no competing financial interest.

■ ACKNOWLEDGMENTS

We thank FRQNT and Aligo Innovation for financial support. The authors would like to thank Prof. Sylvain Canesi (UQAM) and Chloe L'homme for training in the synthesis of FcDMPE; Prof. Scott Bohle (McGill) for helpful discussions; and Adam Elmerikhi for a generous gift of materials.

■ ABBREVIATIONS

DDS = drug delivery system
FcDMPE = ferrocene-modified phospholipid
FTDMA = ferrocene-modified quaternary ammonium amphiphile
BZQ = 1,4-benzoquinone
EPR = enhanced permeability and retention

■ REFERENCES

(1) Gregoriadis, G. Liposome Research in Drug Delivery: The Early Days. *J. Drug Target.* **2008**, *16* (7−8), 520−524.
(2) Bouwstra, J. A.; Honeywell-Nguyen, P. L. Skin Structure and Mode of Action of Vesicles. *Adv. Drug Delivery Rev.* **2002**, *54*, S41−S55.
(3) Goins, B. A.; Phillips, W. T. The Use of Scintigraphic Imaging as a Tool in the Development of Liposome Formulations. *Prog. Lipid Res.* **2001**, *40* (1−2), 95−123.
(4) Bulbake, U.; Doppalapudi, S.; Kommineni, N.; Khan, W. Liposomal Formulations in Clinical Use: An Updated Review. *Pharmaceutics* **2017**, *9* (4), 12−33.
(5) Weissig, V.; Pettinger, T. K.; Murdock, N. Nanopharmaceuticals (Part 1): Products on the Market. *Int. J. Nanomed.* **2014**, *9*, 4357−4373.
(6) Noyhouzer, T.; L'Homme, C.; Beaulieu, I.; Mazurkiewicz, S.; Kuss, S.; Kraatz, H.-B.; Canesi, S.; Mauzeroll, J. Ferrocene-Modified Phospholipid: An Innovative Precursor for Redox-Triggered Drug Delivery Vesicles Selective to Cancer Cells. *Langmuir* **2016**, *32*, 4169−4178.
(7) Fischer, A.; Oberholzer, T.; Luisi, P. L. Giant Vesicles as Models to Study the Interactions between Membranes and Proteins. *Biochim. Biophys. Acta, Biomembr.* **2000**, *1467* (1), 177−188.
(8) Walde, P.; Cosentino, K.; Engel, H.; Stano, P. Giant Vesicles: Preparations and Applications. *ChemBioChem* **2010**, *11* (7), 848−865.
(9) Kobayashi, H.; Watanabe, R.; Choyke, P. L. Improving Conventional Enhanced Permeability and Retention (EPR) Effects; What Is the Appropriate Target? *Theranostics* **2014**, *4* (1), 81−89.
(10) Matsumura, Y.; Maeda, H. A New Concept for Macromolecular Therapeutics in Cancer Chemotherapy: Mechanism of Tumoritropic Accumulation of Proteins and the Antitumor Agents Smancs. *Cancer Res.* **1986**, *46*, 6387−6392.
(11) Nichols, J. W.; Han Bae, Y. EPR: Evidence and Fallacy. *J. Controlled Release* **2014**, *190*, 451−464.
(12) Danhier, F. To Exploit the Tumor Microenvironment: Since the EPR Effect Fails in the Clinic, What Is the Future of Nanomedicine? *J. Controlled Release* **2016**, *244*, 108−121.

DOI: 10.1021/acs.langmuir.8b04267
Langmuir 2019, 35, 5608−5616

(13) Rosenblum, D.; Joshi, N.; Tao, W.; Karp, J. M.; Peer, D. Progress and Challenges towards Targeted Delivery of Cancer Therapeutics. *Nat. Commun.* **2018**, *9* (1), 1410.
(14) Zanoni, M.; Piccinini, F.; Arienti, C.; Zamagni, A.; Santi, S.; Polico, R.; Bevilacqua, A.; Tesei, A. 3D Tumor Spheroid Models for in Vitro Therapeutic Screening: A Systematic Approach to Enhance the Biological Relevance of Data Obtained. *Sci. Rep.* **2016**, *6*, 1−11.
(15) Blanco, E.; Shen, H.; Ferrari, M. Principles of Nanoparticle Design for Overcoming Biological Barriers to Drug Delivery. *Nat. Biotechnol.* **2015**, *33* (9), 941−951.
(16) Lasic, D. D.; Martin, F. J. On the Mechanism of Vesicle Formation. *J. Membr. Sci.* **1990**, *50* (2), 215−222.
(17) Cantor, R. S. Lipid Composition and the Lateral Pressure Profile in Bilayers. *Biophys. J.* **1999**, *76* (5), 2625−2639.
(18) Cantor, R. S. The Lateral Pressure Profile in Membranes: A Physical Mechanism of General Anesthesia. *Biochemistry* **1997**, *36* (9), 2339−2344.
(19) Hafez, I. M.; Ansell, S.; Cullis, P. R. Tunable PH-Sensitive Liposomes Composed of Mixtures of Cationic and Anionic Lipids. *Biophys. J.* **2000**, *79* (3), 1438−1446.
(20) Ellens, H.; Bentz, J.; Szoka, F. C. Fusion of Phosphatidylethanolamine-Containing Liposomes and Mechanism of the La-Hn Phase Transition1. *Biochemistry* **1986**, *25*, 4141−4147.
(21) Guo, X.; MacKay, J. A.; Szoka, F. C. Mechanism of PH-Triggered Collapse of Phosphatidylethanolamine Liposomes Stabilized by an Ortho Ester Polyethyleneglycol Lipid. *Biophys. J.* **2003**, *84* (3), 1784−1795.
(22) Ong, W.; Yang, Y.; Cruciano, A. C.; McCarley, R. L. Redox-Triggered Contents Release from Liposomes. *J. Am. Chem. Soc.* **2008**, *130* (44), 14739−14744.
(23) Mcmaster, M. L.; Kristinsson, S. Y.; Turesson, I.; Bjorkholm, M.; Landgren, O. Release Rates of Liposomal Contents Are Controlled by Kosmotropes and Chaotropes. *Clin. Lymphoma Myeloma* **2009**, *9* (1), 19−22.
(24) Loew, M.; Forsythe, J. C.; McCarley, R. L. Lipid Nature and Their Influence on Opening of Redox-Active Liposomes. *Langmuir* **2013**, *29* (22), 6615−6623.
(25) Itoh, S. SURFACE POTENTIAL AND REACTION OF THE MEMBRANE-BOUND ELECTRON TRANSFER COMPONENTS II. INTEGRITY OF THE CHLOROPLAST MEMBRANE AND REACTION OF P-700. *Biochim. Biophys. Acta, Bioenerg.* **1979**, *548*, 596−607.
(26) Yao, W. W.; Lau, C.; Hui, Y.; Poh, H. L.; Webster, R. D. Electrode-Supported Biomembrane for Examining Electron-Transfer and Ion-Transfer Reactions of Encapsulated Low Molecular Weight Biological Molecules. *J. Phys. Chem. C* **2011**, *115* (5), 2100−2113.
(27) Cram, D. J.; Reeves, R. A. Macro Rings. XIV. Substitution Studies in the [4.4]Paracyclophane System. *J. Am. Chem. Soc.* **1958**, *80* (12), 3094−3103.
(28) Stewart, J. C. M. Colorimetric Determination of Phospholipids with Ammonium Ferrothiocyanate. *Anal. Biochem.* **1980**, *104* (1), 10−14.
(29) Saji, T.; Hoshino, K.; Aoyagui, S. Reversible Formation and Disruption of Micelles by Control of the Redox State of the Surfactant Tail Group. *J. Chem. Soc., Chem. Commun.* **1985**, No. 13, 865.
(30) Danis, L.; Polcari, D.; Kwan, A.; Gateman, S. M.; Mauzeroll, J. Fabrication of Carbon, Gold, Platinum, Silver, and Mercury Ultramicroelectrodes with Controlled Geometry. *Anal. Chem.* **2015**, *87* (5), 2565−2569.
(31) Herrera, F. E.; Bouchet, A.; Lairion, F.; Disalvo, E. A.; Pantano, S. Molecular Dynamics Study of the Interaction of Arginine with Phosphatidylcholine and Phosphatidylethanolamine Bilayers. *J. Phys. Chem. B* **2012**, *116* (15), 4476−4483.
(32) Andreussi, O.; Dabo, I.; Marzari, N. Revised Self-Consistent Continuum Solvation in Electronic-Structure Calculations. *J. Chem. Phys.* **2012**, *136* (6), 064102.
(33) Hutter, J.; Iannuzzi, M.; Schiffmann, F.; Vandevondele, J. Cp2k: Atomistic Simulations of Condensed Matter Systems. *Wiley Interdiscip. Rev. Comput. Mol. Sci.* **2014**, *4* (1), 15−25.
(34) VandeVondele, J.; Hutter, J. Gaussian Basis Sets for Accurate Calculations on Molecular Systems in Gas and Condensed Phases. *J. Chem. Phys.* **2007**, *127* (11), 114105.
(35) Goedecker, S.; Teter, M. Separable Dual-Space Gaussian Pseudopotentials. *Phys. Rev. B: Condens. Matter Mater. Phys.* **1996**, *54* (3), 1703−1710.
(36) Krack, M. Pseudopotentials for H to Kr Optimized for Gradient-Corrected Exchange-Correlation Functionals. *Theor. Chem. Acc.* **2005**, *114* (1−3), 145−152.
(37) Perdew, J. P.; Burke, K.; Ernzerhof, M. Generalized Gradient Approximation Made Simple. *Phys. Rev. Lett.* **1996**, *77* (18), 3865−3868.
(38) Grimme, S.; Antony, J.; Ehrlich, S.; Krieg, H. A Consistent and Accurate Ab Initio Parametrization of Density Functional Dispersion Correction (DFT-D) for the 94 Elements H-Pu. *J. Chem. Phys.* **2010**, *132* (15), 154104.
(39) Mccarley, R. L. Redox-Responsive Delivery Systems. *Annu. Rev. Anal. Chem.* **2012**, *5*, 391−411.
(40) Vulugundam, G.; Kumar, K.; Kondaiah, P.; Bhattacharya, S. Efficacious Redox-Responsive Gene Delivery in Serum by Ferrocenylated Monomeric and Dimeric Cationic Cholesterols. *Org. Biomol. Chem.* **2015**, *13* (14), 4310−4320.
(41) Muller, J. P. E.; Aytar, B. S.; Kondo, Y.; Lynn, D. M.; Abbott, N. L. Incorporation of DOPE into Lipoplexes Formed from a Ferrocenyl Lipid Leads to Inverse Hexagonal Nanostructures That Allow Redox-Based Control of Transfection in High Serum. *Soft Matter* **2012**, *8* (24), 6608−6619.
(42) Kumar, K.; Vulugundam, G.; Kondaiah, P.; Bhattacharya, S. Co-Liposomes of Redox-Active Alkyl-Ferrocene Modified Low MW Branched PEI and DOPE for Efficacious Gene Delivery in Serum. *J. Mater. Chem. B* **2015**, *3*, 2318−2330.
(43) Saji, T.; Hoshino, K.; Aoyagui, S. Reversible Formation and Disruption of Micelles by Control of the Redox State of the Head Group. *J. Am. Chem. Soc.* **1985**, *107* (24), 6865−6868.
(44) Ahonen, P.; Ruiz, V.; Kontturi, K.; Liljeroth, P.; Quinn, B. M. Electrochemical Gating in Scanning Electrochemical Microscopy. *J. Phys. Chem. C* **2008**, *112* (7), 2724−2728.
(45) Bangham, A. D.; Standish, M. M.; Watkins, J. C. Diffusion of Univalent Ions across the Lamellae of Swollen Phospholipids. *J. Mol. Biol.* **1965**, *13* (1), 238−IN27.
(46) Reeves, J. P.; Dowben, R. M. Formation and Properties of Thin-Walled Phospholipid Vesicles. *J. Cell. Physiol.* **1969**, *73* (1), 49−60.
(47) LIPEX 10/1.5mL Thermobarrel and Regular Barrel Extruder Assembly and Operating Manual. http://www.transferra.ca/wp-content/uploads/2016/03/LIPEX-1.5-and-10mL-Extruder-Operating-Manual-version-2.0.0-2016.pdf.
(48) Mini-Extruder Extrusion Technique. https://avantilipids.com/divisions/equipment-products/mini-extruder-extrusion-technique.
(49) Fenske, D. B.; Cullis, P. R. *Liposome Technology, Vol 2_CRC*, 3rd ed.; Gregoriadis, G., Ed.; Informa Healthcare USA, Inc, 1984; Vol. *II*.
(50) Cecil, R.; Littler, J. S.; Easton, G. Electron Transfer Oxidation of Organic Compounds. Part 111. Oxidation of Cyclohexanone by the Hexachloroiridate(Iv) Anion and by Related Species. *J. Chem. Soc. B* **1970**, 626−631.
(51) Sridharan, V.; Mene, J. C. Cerium (IV) Ammonium Nitrate as a Catalyst in Organic Synthesis. *Chem. Rev.* **2010**, *110*, 3805−3849.
(52) Bard, A. J.; Faulkner, L. R. *Electrochemical Methods: Fundamentals and Applications*, 2nd ed.; Harris, D., Swain, E., Robey, C., Aiello, E., Eds.; John Wiley & Sons: New York, 2001.
(53) Bolton, J. L.; Dunlap, T. Formation and Biological Targets of Quinones: Cytotoxic versus Cytoprotective Effects. *Chem. Res. Toxicol.* **2017**, *30* (1), 13−37.
(54) Connelly, N. G.; Geiger, W. E. Chemical Redox Agents for Organometallic Chemistry. *Chem. Rev.* **1996**, *96* (2), 877−910.
(55) Peover, M. E. A Polarographic Investigation into the Redox Behaviour of Quinones: The Roles of Electron Affinity and Solvent. *J. Chem. Soc.* **1962**, 4540−4549.

DOI: 10.1021/acs.langmuir.8b04267
Langmuir 2019, 35, 5608−5616

(56) Singh, S. K.; Husain, S. M. A Redox-Based Superoxide Generation System Using Quinone/Quinone Reductase. *ChemBioChem* **2018**, *19* (15), 1657−1663.
(57) Gligorovski, S.; Strekowski, R.; Barbati, S.; Vione, D. Environmental Implications of Hydroxyl Radicals (•OH). *Chem. Rev.* **2015**, *115* (24), 13051−13092.
(58) Morante, A.; Forteza, R.; CerdÁ, V. Potassium Nitrosodisulphonate (Fremy's Salt) as a New Redox Thermometric Titrant. *Thermochim. Acta* **1987**, *118* (C), 215−222.
(59) Miranda, K. M. The Chemistry of Nitroxyl (HNO) and Implications in Biology. *Coord. Chem. Rev.* **2005**, *249* (3−4), 433−455.
(60) Paolocci, N.; Dutton, A. S.; Fukuto, J. M.; Bartberger, M. D.; Houk, K. N.; Wink, D. A. The Physiological Chemistry and Biological Activity of Nitroxyl (HNO): The Neglected, Misunderstood, and Enigmatic Nitrogen Oxide. *Chem. Res. Toxicol.* **2005**, *18* (5), 790−801.
(61) Grélard, A.; Loudet, C.; Diller, A.; Dufourc, E. J. *Membrane Protein Structure Determination: Methods and Protocols*; Lacapère, J., Ed.; Humana Press, 2010.
(62) Cevc, G. How Membrane Chain-Melting Phase-Transition Temperature Is Affected by the Lipid Chain Asymmetry and Degree of Unsaturation: An Effective Chain-Length Model. *Biochemistry* **1991**, *30* (29), 7186−7193.
(63) Guin, P. S.; Das, S.; Mandal, P. C. Electrochemical Reduction of Quinones in Different Media: A Review. *Int. J. Electrochem.* **2011**, *2011*, 1−22.
(64) Zimmer, H.; Lankin, D. C.; Horgan, S. W. Oxidations with Potassium Nitrosodisulfonate (Fremy's Radical). The Teuber Reaction. *Chem. Rev.* **1971**, *71* (2), 229−246.

DOI: 10.1021/acs.langmuir.8b04267
Langmuir 2019, 35, 5608−5616